Disentangling $4f$-radical coupling and dissipative Landau-Zener quantum tunneling in a continuously measured single-ion magnet spin transistor

Kieran Hymas and Alessandro Soncini*
School of Chemistry, University of Melbourne, Parkville, Victoria 3010, Australia

(Received 29 September 2021; revised 4 November 2021; accepted 8 November 2021; published 17 November 2021)

Both radical-lanthanide exchange coupling and crystal-field tunnel splitting are responsible for the ground to first-excited Kramers doublet energy gap $\Delta E_{\rm KD}$ in an Ising $4f$ single-ion magnet coupled to a noninnocent ligand. However, these two mechanisms cannot be easily disentangled via spectroscopy alone because their interplay results in a single absorption line. Here we present a microscopic theory for the continuous measurement of the dissipative Landau-Zener transitions recently discussed for a $TbPc_2$ spin transistor [Phys. Rev. Lett. **118**, 257701 (2017)] and show how this quantum transport experiment can be used to disentangle the magnetic coupling and the tunnel splitting contributions to $\Delta E_{\rm KD}$. In addition, our model elucidates the microscopic origin of the decoherent spin tunneling observed in the $TbPc_2$ spin transistor, by explicitly exposing the role played by phonon-mediated spin relaxation and sequential electron transport through the noninnocent ligand, in a time-dependent magnetic field.

DOI: 10.1103/PhysRevB.104.205306

I. INTRODUCTION

Lanthanide-containing single-molecule magnets (SMMs) have come to the forefront of research in molecular magnetism owing to their large magnetic anisotropy barriers [1,2], high blocking temperatures [3–5], and novel implementations in next-generation molecular electronic devices [6–12]. The sizable magnetic anisotropy of lanthanide-containing SMMs (juxtaposed with transition-metal SMMs) originates from strong spin-orbit coupling of electrons in the lanthanide $4f$ shell, leading to thermally well-isolated ground spin-orbit multiplets, whose degeneracy is lifted by comparatively weak electrostatic interactions with surrounding ligands [13]. For even (odd) $4f$-electron systems exhibiting strong easy-axis anisotropy, the axial component of the crystal-field potential splits the Ln ground multiplet with total angular-momentum quantum number J in well-separated Ising (Kramers) doublets $|\pm m_J\rangle$, which can give rise to particularly large energetic barriers to the reversal of the molecular magnetization; generally spanning $\geqslant 10^3$ cm^{-1}. For Ising-type Ln ions in particular, the weaker nonaxial crystal-field contributions can couple the degenerate $|\pm m_J\rangle$ components of an Ising doublet in high-order perturbation theory, resulting in the zero-field tunneling ground state $\frac{1}{\sqrt{2}}(|-m_J\rangle - |m_J\rangle)$ separated from $\frac{1}{\sqrt{2}}(|-m_J\rangle + |m_J\rangle)$ by a tunnel splitting Δ. As a consequence, quantum tunneling of the magnetization (QTM) readily short-circuits the energetic barrier to magnetic relaxation and leads to poor SMM properties. In a bid to suppress zero-field QTM in non-Kramers Ln SMMs, a radical-containing ligand may be incorporated into the molecule rendering the SMM a Kramers system, in which ligand-field induced QTM within the ground-state Kramers doublet is forbidden with no applied magnetic field [14,15].

For the rational design of non-Kramers SMMs with noninnocent ligands, experimental access to the Ln-radical exchange coupling $a_{\rm ex}$ can be useful. Electron paramagnetic resonance (EPR) studies have previously been employed to address this coupling by probing transitions between the ground and first-excited Kramer's doublets of the Ln-radical system [16–19]. Treating the tunnel splitting Δ of the Ising-ion ground doublet on the same footing as the Ln-radical exchange, the magnitude of the energy gap between the resulting Kramers doublets follows from the effective Hamiltonian $H_{\rm eff} = -a_{\rm ex} J_z s_z + \Delta^* |m_J\rangle\langle -m_J| + \text{H.c.}$, diagonalized on the basis of the four product states formed from the radical spin doublet $|\pm\frac{1}{2}\rangle$, and the $|\pm m_J\rangle$ ground Ising doublet of the Ln ion:

$$\Delta E_{\rm KD} = \sqrt{(a_{\rm ex} m_J)^2 + 4\Delta^2}. \tag{1}$$

Since both Ln-radical exchange and tunnel splitting contribute to the energy gap, spectroscopic methods which only probe $\Delta E_{\rm KD}$ are unlikely to disentangle the two mechanisms at play and provide an unambiguous measurement of $a_{\rm ex}$.

A SMM molecular spintronics device operating in the Coulomb blockade regime (where the redox state of the ligand, hence the presence of a radical on the ligand, may be controlled through a gate electrode) offers a natural experimental setup for disentangling the contributions of the exchange coupling and the intrinsic tunnel splitting of the non-Kramers ion to the electronic structure of a Ln-radical SMM (see Fig. 1) [20]. In fact, in a joint experimental and theoretical work, Troiani *et al.* investigated the tunnel-splitting-dependent spin reversal dynamics of $TbPc_2$ in a three-terminal transistor geometry as a function of sweeping magnetic field [21]. A marked deviation in the spin reversal probability behavior of the device was observed rather than that predicted by the traditional Landau-Zener theory for a closed quantum system [22–25]. To uncover the origin of the quite

*asoncini@unimelb.edu.au

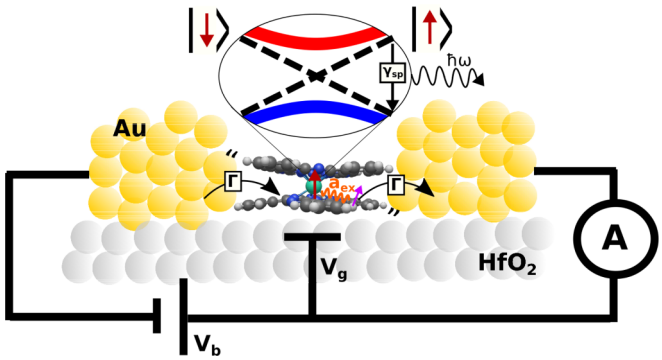

FIG. 1. Schematic of the single-molecule magnet-based molecular spin transistor investigated in the proceeding text. $TbPc_2$ is contacted with a broken Au nanowire that forms the electronic leads of the device mounted on a HfO_2 substrate and facilitates the reduction of the phthalocyaninato ligands with a radical (purple arrow) at a rate Γ by the application of a bias voltage V_b. The magnetic moment of Tb^{3+} (red arrow) is exchange coupled to this radical by a_{ex} as well as to lattice vibrations in the substrate. The inset illustrates the time evolution of the lowest-lying adiabatic states (solid lines) and the diabatic states (dashed lines) of the $TbPc_2$ $^7F_6$ multiplet when a magnetic field is traced across the device. The direct relaxation between these adiabats proportional to γ_{sp} is shown schematically as the emission of an acoustic phonon to the substrate.

different reversal dynamics, a Lindblad-type master equation was employed and found best agreement with experimental measurements when the adiabatic Lindblad operators were expressed as averages over a phenomenological timescale τ_{av}. The timescale τ_{av} was interpreted as the finite time-resolution of each conductance measurement that switched the role of the Lindblad operators to an adiabatic (diabatic) dephasing operator when the tracing velocity was faster (slower) than τ_{av}. While this theoretical approach provides some intuition into the reversal dynamics of the device, the lack of a microscopic modeling of the dephasing of the $4f$ quantum states leaves as an open question the extent to which the decoherence originates from environment-mediated spin relaxation or from the measurement procedure itself, and thus to what degree the experimental measurements depend on the electronic structure of the molecule.

In this paper, we first present a quantum master-equation representation of the $TbPc_2$ break junction spin dynamics replete with a microscopic modeling of both charge transfer and phonon relaxation mechanisms. We highlight three distinct regimes of spin dynamics in which the $TbPc_2$ Ising ground spin is affected by various relaxation processes triggered at different sweeping velocities of the tracing magnetic field. As a result, we provide a microscopic interpretation of the timescale τ_{av} as inversely proportional to the proper two-step sequential charging and discharging rates associated with the electrical, magnetic moment readout of the $TbPc_2$ $4f$ quantum states. Lastly, we use our microscopic model to study the SMM spin reversal dynamics as a function of tunnel splitting and field sweeping domain leading to a proposal for the extraction of Δ and a_{ex} in a general Ising $4f$-radical coupled magnet using a molecular spintronics setup.

II. THEORETICAL MODEL

Keeping the $TbPc_2$ molecular break junction device in mind, we model a SMM-molecular spintronics device as a quantum spin system that is driven by a tracing magnetic field and coupled via ligand field distortions to a dissipative phonon bath while also being allowed to exchange electrons with two semi-infinite source and drain electron reservoirs (leads). We assume here that electron transfer between the molecule and leads occurs via the LUMO of the radical-hosting ligands such that they form a readout quantum dot, as is the case for $TbPc_2$ [26,27]. Accordingly, the time-dependent Hamiltonian for the entire system can be partitioned as $H(t) = H_S(t) + H_{ph} + H_L + H_{sp} + H_T$, which accounts for the spin system, phonon bath, electronic leads, spin-phonon coupling, and electron tunneling, respectively.

The phonon bath originates from lattice vibrations within the device substrate and is assumed to be in equilibrium. Its spectrum is represented by $H_{ph} = \sum_{\mathbf{q}} \hbar\omega_{\mathbf{q}} b^\dagger_{\mathbf{q}} b_{\mathbf{q}}$ where $b^{(\dagger)}_{\mathbf{q}}$ are bosonic (creation) annihilation operators that (create) destroy phonons with wave vector $\mathbf{q}$ and frequency $\omega_{\mathbf{q}}$. To account for magnetoelastic interactions between the angular-momentum states of the single-molecule magnet and acoustic phonons in the device substate, we introduce a model Hamiltonian that induces transitions between the $4f$ quantum states of the magnet via distortions of its ligand field with

$$H_{sp} = \sum_{\mathbf{q}} \left.\frac{\partial H_{cf}}{\partial Q_{\mathbf{q}}}\right|_0 Q_{\mathbf{q}}, \tag{2}$$

where $Q_{\mathbf{q}}$ is the contribution of the active mode of vibration of the molecule to the device phonon eigenmode with wave vector $\mathbf{q}$ and H_{cf} is the crystal-field Hamiltonian for $TbPc_2$ grafted to the break junction [28].

The leads Hamiltonian $H_L = \sum_{\alpha\mathbf{k}\sigma} \epsilon_{\alpha\mathbf{k}\sigma} a^\dagger_{\alpha\mathbf{k}\sigma} a_{\alpha\mathbf{k}\sigma}$ describes two reservoirs (labeled $\alpha = S, D$) of noninteracting electrons with wave vectors $\mathbf{k}$, spin σ, and energy $\epsilon_{\alpha\mathbf{k}\sigma}$. The operators $a^{(\dagger)}_{\alpha\mathbf{k}\sigma}$ form a set of (creation) annihilation operators that work on the single-particle states $|\alpha\mathbf{k}\sigma\rangle$ of each electrode. Electron exchange between the electronic leads and the phthalocyaninato ligands comprising the readout dot is accounted for by using an Anderson Hamiltonian $H_T = \sum_{\alpha\mathbf{k}\sigma} T^*_{\alpha\mathbf{k}\sigma} a^\dagger_{\alpha\mathbf{k}\sigma} c_\sigma + T_{\alpha\mathbf{k}\sigma} c^\dagger_\sigma a_{\alpha\mathbf{k}\sigma}$ where $c^{(\dagger)}_\sigma$ annihilates (creates) an electron with spin σ from (on) the readout dot and the $T_{\alpha\mathbf{k}\sigma}$ are lead-dot hopping amplitudes.

Without loss of generality, we consider a Ln SMM with a ground $|m_J = \pm J\rangle$ doublet that is energetically well-isolated from other $|m_J\rangle$ states in the ground spin-orbit multiplet (a reasonable assumption for $T \approx 0.01$ K typical of a molecular spintronics experiment). The Hamiltonian for the nanomagnet exchange coupled to a readout quantum dot and driven by a longitudinal magnetic field is

$$H_S(t) = \sum_\sigma (\varepsilon - eV_g) n_\sigma + V_{tun} - a_{ex} J_z s_z + (g_J J_z + g s_z)\mu_B \frac{dB}{dt}\left(t - \frac{T}{2}\right). \tag{3}$$

In Eq. (3), $n_\sigma = c^\dagger_\sigma c_\sigma$ is the number operator for spin σ electrons occupying the lowest unoccupied molecular orbital (LUMO) of the readout dot with an energy ε that may be

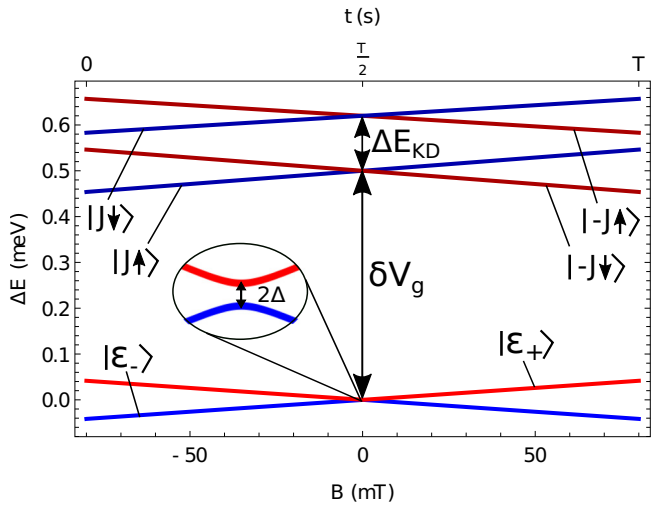

FIG. 2. Zeeman diagram for the lowest-lying states of the $TbPc_2$ molecular break junction obtained from diagonalization of Eq. (3) with gate detuning $\delta V_g = 0.5$ mV. In the field tracing domain ± 80 mT, the reduced states approximately retain the good quantum numbers $|m_J = \pm J, \sigma\rangle$ and are labeled as such. The neutral states are time-varying linear combinations of $|m_J = \pm J\rangle$ and are labeled $|\epsilon_\pm\rangle$.

modified by the application of a gate voltage $V_g = V_g^{(0)} + \delta V_g$ (here $V_g^{(0)}$ brings the ferromagnetic reduced states of the device to level degeneracy with the neutral states). The second term in Eq. (3) accounts for tunneling between the ground states of the Ising ion. For example, a tunnel splitting between the bistable $|\pm J\rangle$ $TbPc_2$ ground states arises, even in the most symmetric crystal structure (D_4), in third-order perturbation theory of the ligand field term $\beta A_4^4 \langle r^4\rangle O_4^4(\mathbf{J})$ [29]. We include the coherent mixing of the Ln ground states effectively as

$$V_{\rm tun} = \Delta |J\rangle\langle -J| + \Delta^* |-J\rangle\langle J|. \tag{4}$$

The penultimate term in Eq. (3) represents the exchange coupling between the Ising-type Ln $4f$ quantum states and a radical spin delocalized in the ligands. The final term represents the Zeeman interaction between the Ln-radical coupled spin states and a tracing, longitudinal magnetic field evolving linearly from $-B_{\rm max}$ to $B_{\rm max}$ at a velocity $\frac{dB}{dt}$. Here, μ_B is the Bohr magneton, $g = 2$ is the bare electron g factor, $s_z = (1/2)[\sigma_z]_{\gamma\gamma'} c_\gamma^\dagger c_{\gamma'}$ is the spin projection operator for the readout dot, g_J is the Landé g factor for the ground doublet of the Ln ion, and J_z is the total angular-momentum projection operator restricted to work only on the $|m_J\rangle$ total angular-momentum states of the ligand field-split ground multiplet. The Hamiltonian presented in Eq. (3) is diagonalized on the product basis of the $|m_J = \pm J\rangle$ ground Ising doublet and the radical spin states $|\sigma = \pm\frac{1}{2}\rangle$ to give the eigenstates $\{|\epsilon_\pm(t)\rangle,\ |\epsilon_{\pm,\sigma}(t)\rangle\}$ with adiabatic energies plotted in Fig. 2. The adiabatic eigenstates for the neutral device are $|\epsilon_\pm(t)\rangle = a_\pm(t)|J\rangle + b_\pm(t)|-J\rangle$, where

$$a_\pm(t) = \frac{1}{\sqrt{2}} \frac{\mathcal{J}(t) + \epsilon_\pm(t)}{\sqrt{\mathcal{J}(t)^2 + \Delta^2 + \mathcal{J}(t)\epsilon_\pm(t)}},$$
$$b_\pm(t) = \frac{1}{\sqrt{2}} \frac{|\Delta|}{\sqrt{\mathcal{J}(t)^2 + \Delta^2 + \mathcal{J}(t)\epsilon_\pm(t)}}. \tag{5}$$

Here, $\mathcal{J}(t) = \mu_B g_J J \frac{dB}{dt}(t - \frac{T}{2})$ and the adiabatic energies are simply $\epsilon_\pm(t) = \pm[\mathcal{J}(t)^2 + |\Delta|^2]^{1/2}$. Owing to the simple Ising coupling of the radical to the nanomagnet ground doublet, the Hamiltonian presented in Eq. (3) does not mix states with different radical spin. The adiabatic states of the reduced manifold are thus $|\epsilon_{\pm,\sigma}(t)\rangle = (a_{\pm,\sigma}(t)|J\rangle + b_{\pm,\sigma}|-J\rangle) \otimes |\sigma\rangle$ with

$$a_{\pm,\sigma}(t) = \frac{1}{\sqrt{2}} \frac{\mathcal{J}_\sigma(t) + Q_{\pm,\sigma}(t)}{\sqrt{\mathcal{J}_\sigma(t)^2 + \Delta^2 + \mathcal{J}_\sigma(t) Q_{\pm,\sigma}(t)}},$$
$$b_{\pm,\sigma}(t) = \frac{1}{\sqrt{2}} \frac{|\Delta|}{\sqrt{\mathcal{J}_\sigma(t)^2 + \Delta^2 + \mathcal{J}_\sigma(t) Q_{\pm,\sigma}(t)}}, \tag{6}$$

and adiabatic energies $\epsilon_{\pm,\sigma}(t) = \varepsilon - eV_g + g\mu_B \frac{dB}{dt}(t - T/2) \pm [\mathcal{J}_\sigma(t)^2 + \Delta^2]^{1/2}$ where $\mathcal{J}_\sigma(t) = \mu_B g_J J \frac{dB}{dt}(t - \frac{T}{2}) - a_{\rm ex} J\sigma$ and $Q_{\pm,\sigma}(t) = \pm[\mathcal{J}_\sigma(t)^2 + \Delta^2]^{1/2}$.

Notably, in the field sweeping domain -80 mT $\leqslant B \leqslant$ 80 mT, the $|\epsilon_{\pm,\sigma}(t)\rangle$ states from the reduced manifold approximately retain their quantum numbers $|m_J, \sigma\rangle$ provided that $a_{\rm ex} \gg \Delta$. Avoided crossings do eventually occur between reduced states hosting a radical of the same spin at $B_{\rm ac} = \frac{a_{\rm ex}\sigma}{g_J \mu_B}$, where the reduced states become linear combinations of the Ising spin $|\epsilon_{\pm,\sigma}(B_{\rm ac})\rangle = \frac{1}{\sqrt{2}}(|J\rangle \pm |-J\rangle) \otimes |\sigma\rangle$.

Throughout this paper we use a gate voltage $V_g = V_g^{(0)} + \delta V_g$ where $V_g^{(0)}$ brings the ferromagnetically coupled reduced states and the neutral states of the device to level degeneracy when no magnetic field is present, thus rendering ε as an arbitrary parameter. The evolution of the adiabatic energies under a linear magnetic field trace and a detuning $\delta V_g = 0.5$ mV is presented in Fig. 2. We use $\delta V_g = 0.5$ mV in accordance with the experimental setup described in Ref. [21].

To properly account for the influence of charge transport and spin-phonon coupling on the spin dynamics of the single-molecule magnet device during a magnetic-field trace, the Hamiltonians H_T and $H_{\rm sp}$ are treated perturbatively to second order in the von Neumann equation of motion for the density matrix of the entire device $\rho^{\rm tot}(t)$. Notably, since H_T only connects states from different redox manifolds (to first order) while $H_{\rm sp}$ does not, there are no mixed $H_{\rm sp} \times H_T$ terms that appear to second order in the perturbation theory. Following standard manipulations [30,31], we arrive at a set of coupled nonadiabatic master equations for the reduced density matrix of the quantum spin system $[\rho(t) = {\rm Tr}_{L+B}\{\rho^{\rm tot}(t)\}$ defined by tracing over all states in the leads and phonon bath] on the basis of the adiabatic eigenstates of the Hamiltonian provided in Eq. (3). A general matrix element evolves according to

$$\dot\rho_{mn} = \sum_l \langle \dot\epsilon_m|\epsilon_l\rangle \rho_{ln} + \rho_{ml}\langle \epsilon_l|\dot\epsilon_n\rangle - \frac{i}{\hbar}[H_S(t), \rho]_{mn} + (\mathcal{R}\rho)_{mn}, \tag{7}$$

where the dissipative dynamics are codified in the superoperator $\mathcal{R}$. The dissipative part takes the form

$$(\mathcal{R}\rho)_{mn} = \delta_{mn} \sum_l (W^{l\to m} + \Omega^{l\to m})\rho_l - \gamma_{mn}\rho_{mn}, \tag{8}$$

with $\gamma_{mn} = \frac{1}{2}\sum_l W^{m\to l} + W^{n\to l} + \Omega^{m\to l} + \Omega^{n\to l}$, and, notably, each dissipative transition rate acquires an explicit

time-dependence when expressed in the adiabatic basis. Within Eq. (7) we account for three dynamical processes that determine the time evolution of the reduced density matrix elements during field tracing. We include (i) nonadiabatic transitions between the states that are mediated by the off-diagonal elements of the reduced density matrix and are proportional to the geometric Berry terms $\langle \dot{\epsilon}_m | \epsilon_l \rangle$, (ii) sequential charging and discharging events between states from different redox manifolds summed over leads and spin $W^{l\to m} = \sum_{\alpha\sigma} W^{l\to m}_{\alpha\sigma}$ and finally, (iii) direct transitions between states $\Omega^{l\to m}$ associated with phonon absorption and emission from and to the substrate, respectively.

We model sequential tunneling of a spin σ electron from lead α onto the device, and thus a transfer of population from state $|\epsilon_\nu(t)\rangle$ to state $|\epsilon_{\nu',\sigma'}(t)\rangle$, using the golden rule transition rate [27]

$$W^{\nu\to\nu'\sigma'}_{\alpha\sigma} = \frac{\Gamma |c_{\nu,\nu'\sigma'}(t)|^2 \delta_{\sigma\sigma'}}{\pi\hbar} \int \frac{f(\varepsilon-\mu_\alpha)\eta d\varepsilon}{(\varepsilon-(\epsilon_{\nu',\sigma'}(t)-\epsilon_\nu(t)))^2+\eta^2}, \tag{9}$$

where $\Gamma/\hbar = 2\pi D_{\alpha\mathbf{k}\sigma}|T_{\alpha\mathbf{k}\sigma}|^2/\hbar \approx 10^8$ s^{-1} is the lead-dot coupling strength which may be taken as constant over the energy range explored within this study [27,32], $c_{\nu,\nu'\sigma'}(t) = a_\nu(t)a_{\nu',\sigma'}(t) + b_\nu(t)b_{\nu',\sigma'}(t)$ is the time-dependent transition amplitude and $\delta_{\sigma\sigma'}$ accounts for the overlap between the charging electron and the reduced state radical spin. Furthermore, $f(\varepsilon-\mu_\alpha) = \{1+\exp[(\varepsilon-\mu_\alpha)/k_BT]\}^{-1}$ is the Fermi-Dirac distribution of electrons in lead α held at the chemical potential $\mu_\alpha = \pm V_b/2$ by an applied bias voltage at the source and drain electrodes. To account for the finite linewidth of the molecular energy levels of the device (obtained from the coupling of the readout dot to the continuum of states in the leads), we make the wide-band assumption and express the rates as a convolution of the leads' thermal functions with a Lorentzian lineshape centered at the charging energy and broadened by η. In a previous study [27], a broadening factor $\eta = 55$ μeV provided good agreement between many aspects of experiment and our theoretical characterization of the same device, thus we employ the same value of η throughout this paper. The discharging rate $W^{\nu'\sigma'\to\nu}_{\alpha\sigma}$ can be readily obtained from Eq. (9) with the substitution $f(\varepsilon-\mu_\alpha) \mapsto [1-f(\varepsilon-\mu_\alpha)]$.

$TbPc_2$ nanomagnets deposited in molecular spintronics devices can hybridize strongly with longitudinal stretching modes in the device substrate (which are active even at cryogenic temperatures) resulting in a rotation $\delta\phi = \nabla\times\delta u(\mathbf{r})$ about the principal magnetic axis of the Ln SMM [33]. We have previously demonstrated [28] how accounting for these vibronic corrections to the crystal-field Hamiltonian of $TbPc_2$ in the context of a Debye model for acoustic phonons in the substrate leads to a direct mechanism for population exchange between the $|m_J = \pm J\rangle$ bistable ground states of the SMM via the mixing-in of excited states in the ground spin-orbit multiplet with lower angular-momentum projections. We make the assumption of a three-dimensional phonon bath in contact with the SMM, justified by recent experiments on the $TbPc_2$ molecular break junction [21,34] which uncovered a cubic longitudinal magnetic-field dependence on the direct relaxation time T_1 between the quantum $4f$ electronic states. Direct transitions between spin states of the nanomagnet conserving electron number are then mediated by phonon absorption (emission) from (to) the device substrate and are captured within a Debye model with the formula

$$\Omega^{l\to m} = \gamma_{\rm sp} \frac{[\epsilon_m(t)-\epsilon_l(t)]^3}{\exp\{[\epsilon_m(t)-\epsilon_l(t)]/k_BT\}-1}. \tag{10}$$

The matrix elements for direct transitions between the adiabatic states remain approximately constant at fields large enough to activate the direct-transition mechanism and so have been absorbed into the coupling constant $\gamma_{\rm sp}$.

The Berry phase terms in Eq. (7) are given by $\langle \dot{\epsilon}_m|\epsilon_l\rangle = \dot{a}_m(t)a_l(t) + \dot{b}_m(t)b_l(t)$ in terms of the compound indices m and l. When $m = l$ these terms are effectively zero however, when $m \neq l$ they approximate sharp Lorentzian lineshapes centered about the avoided level crossing between the two states. For the neutral states, these nonadiabatic terms allow only a unidirectional population transfer from the adiabatic ground state $|\epsilon_-(t)\rangle$ to the excited state $|\epsilon_+(t)\rangle$ via the coherences $\rho_{\pm,\mp}$ and, since their magnitude scales with the tracing velocity $\frac{dB}{dt}$, induce the nonadiabatic transitions predicted by the Landau-Zener theory of a closed quantum system. The same is true for the reduced states when driven through avoided level crossings at $B_{\rm ac} = \frac{a_{\rm ex}\sigma}{g_J\mu_B}$.

To ascertain the effect of magnetic-field sweep rate on the spin-relaxation dynamics of the SMM magnetic moment we initialize the system in the diabatic ground state $\rho_J(0) = 1$ at $t = 0$ ($-B_{\rm max} = -80$ mT) and numerically integrate Eq. (7) up to $t = T$. The probability of finding the magnetic moment reversed upon completion of the magnetic-field trace is given by $P_{\rm gs} = \rho_{-J}(T) + \rho_{-J,\uparrow}(T) + \rho_{-J,\downarrow}(T)$.

III. SPIN REVERSAL DYNAMICS OF THE MOLECULAR BREAK JUNCTION

To illustrate the utility of our microscopic model, we now specialize in the $TbPc_2$ molecular break junction studied by Troiani *et al.* [21] but now with a full microscopic modeling of charge transport and phonon relaxation. We use a tunneling matrix element $\Delta = 5\times10^{-7}$ meV ≈ 1 μK [29] and an exchange coupling to the radical $a_{\rm ex} = 0.02$ meV, which is in accordance with high-level multireference relativistic *ab initio* calculations [35] and recent models of $TbPc_2$ molecular spintronic devices [27,28].

In Fig. 3 we plot the spin reversal probability $P_{\rm gs}$ obtained over a representative domain of magnetic-field sweeping velocities. Notably, throughout the trace the device is continuously measured with an electrical current, i.e., electron charging and discharging occurs through the molecular readout dot at a rate proportional to Γ, however, *vide infra*, only at the avoided crossing ($t = \frac{T}{2}$) can concurrent charging and discharging transitions transfer population between the $|\epsilon_\pm(t)\rangle$ states. Three distinct regimes of spin dynamics clearly appear, in which the reversal probability tends to zero, is approximately one half, or plateaus to certainty, respectively. We refer to each of these magnetic-field tracing speed regimes as the fast, intermediate, and slow dynamics regimes, respectively.

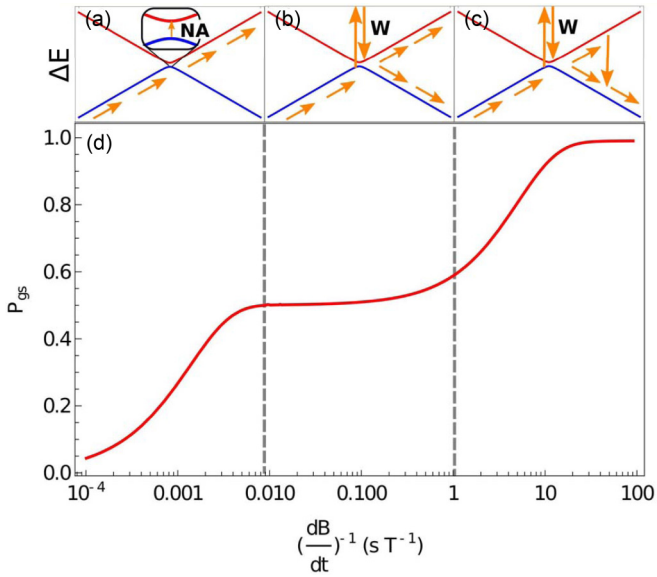

FIG. 3. Schematic diagrams of population evolution (orange arrows) between the adiabatic states of the neutral manifold $|\epsilon_-(t)\rangle$ and $|\epsilon_+(t)\rangle$ in the (a) fast, (b) intermediate, and (c) slow field tracing regimes. (d) Probability for spin reversal P_{gs} of the $TbPc_2$ magnetic moment on completion of the magnetic-field trace ($t = T$) as a function of inverse sweeping rate.

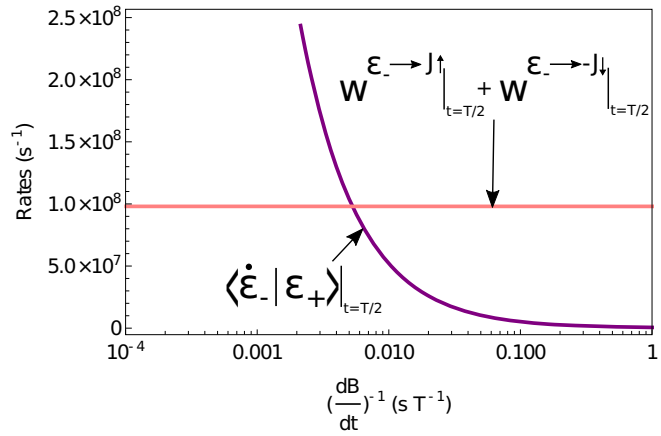

FIG. 4. Value of nonadiabatic Berry terms and charging transition rates evaluated at the avoided level crossing as a function of the inverse of the magnetic-field sweep rate. The nonadiabatic terms become dominant at high sweep rates overtaking the approximately constant charge-transfer equilibration mechanism causing a crossover from the "intermediate" to the "fast" spin dynamics regime at around $(\frac{dB}{dt})^{-1} = 0.005$ s T^{-1}.

In the fast regime, as shown schematically in Fig. 3(a), the dominant mechanism to exchange population between the adiabatic states is the unidirectional nonadiabatic transitions arising from the Berry terms in Eq. (7). As the system passes through the avoided level crossing, population is almost completely transferred from the $|\epsilon_-(t)\rangle$ state to the $|\epsilon_+(t)\rangle$ state (i.e., the Tb^{3+} magnetic moment remains unflipped) followed rapidly by the completion of the field trace and the final measurement of the $TbPc_2$ magnetic moment before any other relaxation process may take place.

The system crosses over from the fast regime to the intermediate regime when the rate of nonadiabatic transitions becomes comparable or weaker than the charge transport transition rates attributed to the continuous conductance measurements through the device (see Fig. 4). When the system is away from the avoided level crossing, the adiabatic states $|\epsilon_\pm(t)\rangle$ are relatively pure (i.e., behave approximately as the diabatic states $|\pm J\rangle$) and thus charging transitions that transfer population to the reduced states (and visa versa) must conserve the total angular momentum of the $TbPc_2$ nanomagnet enforced by the selection rules encoded in the squared matrix element $|c_{\nu,\nu'\sigma'}(t)|^2$ in Eq. (9). At the avoided crossing, however, the adiabatic states are comprised of the symmetric and antisymmetric linear combinations of the diabatic states $|\epsilon_\pm(T/2)\rangle = \frac{1}{\sqrt{2}}(|-J\rangle \pm |J\rangle)$. As a result, at the avoided level crossing the populations of the neutral adiabatic states of the device are equilibrated via two-step charging and discharging transitions to and from the reduced manifold of states which are no longer restricted to conserve the orientation of the $TbPc_2$ magnetic moment; this process is shown schematically in Fig. 3(b). Notably, this environment-assisted equilibration of the populations has been reported in several other works [36–38] where a nonmonotonic behavior of the Landau-Zener probability against sweep velocity is shown to emerge owing to the coupling of the dissipative environment to the quantum system. By studying an enriched model accounting for the coupling of a two-level quantum system to both transversal and longitudinal fluctuations in the dissipative bosonic environment, it was demonstrated that transversal noise caused stronger dissipative effects in the Landau-Zener transition probability than from longitudinal coupling alone [39]. In those works however, the deviation from a coherent Landau-Zener tunneling probability stemmed from a coupling of the quantum-mechanical system to a phonon bath rather than to electronic leads. As in the fast regime, after this equilibration has taken place, the trace is rapidly completed before any other relaxation mechanism affects the spin dynamics of the system resulting in an equal probability of measuring either configuration of the $TbPc_2$ magnetic moment at the final readout. By modeling the continuous measurement of the device as a Coulomb blockade sequential charge-transfer process, we have included microscopically the finite time resolution attributed to the readout mechanism without requiring the introduction of the averaging parameter τ_{av}, as introduced by Troiani *et al.* when modeling the same system [21].

Reducing the field sweeping rate further still, transitions the system to the slow regime of spin reversal dynamics whereby the magnetic moment reversal probability P_{gs} approaches unity coincidental with the adiabatic theorem for closed quantum systems. In the presence of a charge transfer that induces neutral state population equilibration at the avoided crossing however, the means by which this limit is reached relies on a phonon-mediated direct relaxation from the excited state $|\epsilon_+(t)\rangle$ back to the ground state before the trace is complete and the final measurement of the $TbPc_2$ magnetic moment is made. This cascade of events is illustrated schematically in Fig. 3(c).

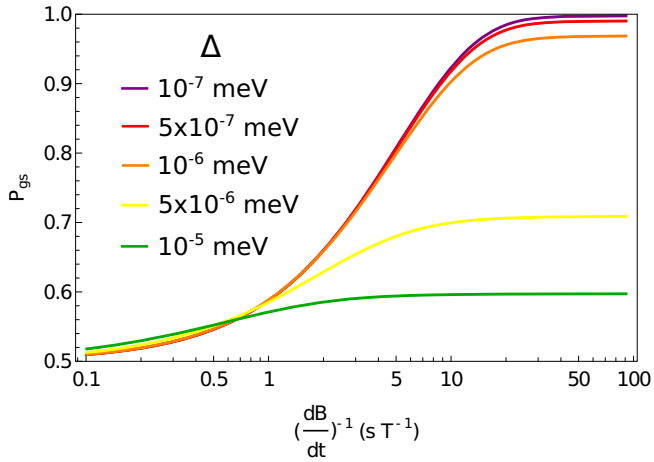

FIG. 5. Probability for spin reversal P_{gs} of the SMM for a representative set of sweeping rates $\frac{dB}{dt}$ on the domain $-80\ \text{mT} \leqslant B \leqslant 80\ \text{mT}$ for various values of tunnel splitting Δ.

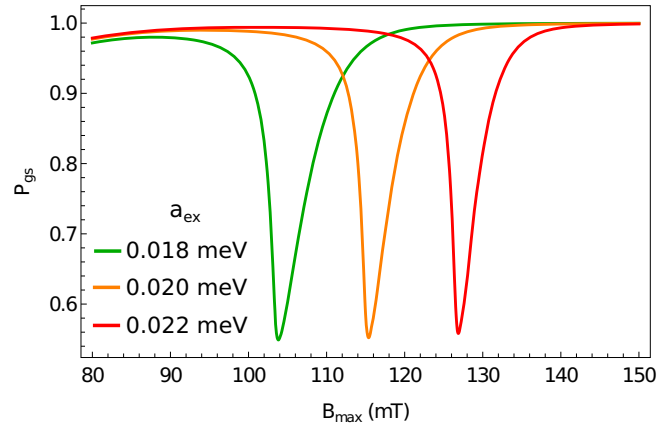

FIG. 6. Probability for spin reversal P_{gs} of the SMM as a function of the sweeping field domain $-B_{\max} \leqslant B \leqslant B_{\max}$ when $\Delta = 5 \times 10^{-7}$ meV, $\frac{dB}{dt} = 0.05\ \text{T s}^{-1}$, and $a_{\text{ex}} = 0.022$ meV (red), 0.02 meV (orange), and 0.018 meV (green).

IV. ELECTRONIC STRUCTURE EFFECTS ON REVERSAL PROBABILITIES

We next explored the spin reversal probability dependence on the tunnel splitting gap Δ. From Fig. 5, we observe a reduction in the slow regime plateau for increased tunnel splitting. As the tunnel splitting becomes larger, the mixing of the diabatic states $|\pm J\rangle$ in $|\epsilon_{\pm}(t)\rangle$ persists for larger regions of the field-sweeping domain. Thus, the restriction of population transfer between the adiabatic states $|\epsilon_{\pm}(t)\rangle$ via the two-step charge transport mechanism is relaxed and may occur throughout the trace (not just at $t = \frac{T}{2}$). The measurement-induced equilibration of the adiabatic populations (that becomes faster for larger Δ) competes with phonon relaxation to the $|\epsilon_{-}(t)\rangle$ ground state leading to a depletion of P_{gs} in the slow regime of spin dynamics.

Up until now, we have focused on the sweeping field domain $-80\ \text{mT} \leqslant B \leqslant 80\ \text{mT}$ wherein the m_J quantum numbers of the reduced states are approximately retained. Extending the sweeping field domain so as to include the avoided crossings in the reduced states (at $B_{\text{ac}} = \frac{a_{\text{ex}}\sigma}{g_J \mu_B}$) introduces a new mechanism for population transfer between the neutral $|\epsilon_{\pm}(t)\rangle$ states since, at these crossings, charge transport processes need not conserve the total angular-momentum quantum number of the Ising system [see Eq. (9)]. Specializing to the slow dynamics regime defined at $B_{\max} = 80$ mT, where phonon emission processes should return the system to the ground state on completion of the trace (i.e., $P_{\text{gs}} = 1$), in Fig. 6 we explore P_{gs} as a function of the field sweeping domain limit $B_{\max}$ for different values of the exchange coupling a_{ex}. While P_{gs} is essentially saturated for most $B_{\max}$, a precipitous drop in the reversal probability occurs at the value of B_{ac}. For $B_{\max} = B_{\text{ac}}$, the final measurement of the SMM spin states equilibrates $|\pm J\rangle$ leaving no time for a phonon emission event, thus $P_{\text{gs}} < 1$. The broadness of this signal is governed by the speed of phonon-mediated relaxation from the excited adiabat and the magnitude of tunnel splitting between the reduced states of the device. The minimum of this signal, however, is located at B_{ac} and hence provides a direct measurement of the SMM-radical exchange coupling.

V. CONCLUSIONS

We have employed a nonadiabatic quantum master-equation approach to uncover the microscopic mechanisms underpinning the spin reversal dynamics of a continuously measured single-molecule magnet molecular break junction while a magnetic field is traced across the device. Focusing on the experimentally realized $TbPc_2$ break junction, we identified three distinct regimes of spin reversal dynamics that originate from the interplay between various population transfer mechanisms and the sweeping velocity of the magnetic field either at an avoided crossing or later during the trace. In the fast regime, unidirectional nonadiabatic transitions become the dominant population transfer process which preserves the initialized orientation of the $TbPc_2$ magnetic moment during the trace. In the intermediate regime, a two-step charge-transfer mechanism associated with the electronic readout measurement out-competes the nonadiabatic transitions and results in a population equilibration of the adiabatic states which is approximately maintained on completion of the trace. The slow regime sees a phonon-assisted direct relaxation event subsequent to the aforementioned population equilibration relaxing the system from its excited state, thus resulting in a complete magnetic moment reversal of the $TbPc_2$ SMM at the final spin state readout.

Using our microscopic model, we explored the reversal probability P_{gs} as a function of tunnel splitting Δ, emphasizing the diminishing saturation value of P_{gs} for slow tracing fields when Δ is large. Lastly, we established a protocol for the measurement of the SMM-radical exchange coupling constant a_{ex}, whereby a local minimum in P_{gs} when extending the field sweeping domain $B_{\max}$ provides a measurement of B_{ac} and consequently, of a_{ex}.

ACKNOWLEDGMENTS

This research was funded by the Australian Research Council Discovery Project No. DP210103208.

[1] H. Wu, M. Li, Z. Xia, V. Montigaud, O. Cador, B. Le Guennic, H. Ke, W. Wang, G. Xie, S. Chen, and S. Gao, High temperature quantum tunnelling of magnetization and thousand kelvin anisotropy barrier in a Dy 2 single-molecule magnet, Chem. Commun. **57**, 371 (2021).

[2] Z. Zhu, C. Zhao, T. Feng, X. Liu, X. Ying, X.-L. Li, Y.-Q. Zhang, and J. Tang, Air-stable chiral single-molecule magnets with record anisotropy barrier exceeding 1800 K, J. Am. Chem. Soc. **143**, 10077 (2021).

[3] C. A. Goodwin, F. Ortu, D. Reta, N. F. Chilton, and D. P. Mills, Molecular magnetic hysteresis at 60 kelvin in dysprosocenium, Nature (London) **548**, 439 (2017).

[4] F. S. Guo, B. M. Day, Y. C. Chen, M. L. Tong, A. Mansikkamäki, and R. A. Layfield, A dysprosium metallocene single-molecule magnet functioning at the axial limit, Angew. Chem. **129**, 11603 (2017).

[5] F. S. Guo, B. M. Day, Y. C. Chen, M. L. Tong, A. Mansikkamäki, and R. A. Layfield, Magnetic hysteresis up to 80 kelvin in a dysprosium metallocene single-molecule magnet, Science **362**, 1400 (2018).

[6] R. Vincent, S. Klyatskaya, M. Ruben, W. Wernsdorfer, and F. Balestro, Electronic read-out of a single nuclear spin using a molecular spin transistor, Nature (London) **488**, 357 (2012).

[7] S. Thiele, F. Balestro, R. Ballou, S. Klyatskaya, M. Ruben, and W. Wernsdorfer, Electrically driven nuclear spin resonance in single-molecule magnets, Science **344**, 1135 (2014).

[8] C. Godfrin, A. Ferhat, R. Ballou, S. Klyatskaya, M. Ruben, W. Wernsdorfer, and F. Balestro, Operating Quantum States in Single Magnetic Molecules: Implementation of Grover's Quantum Algorithm, Phys. Rev. Lett. **119**, 187702 (2017).

[9] C. Godfrin, R. Ballou, E. Bonet, M. Ruben, S. Klyatskaya, W. Wernsdorfer, and F. Balestro, Generalized Ramsey interferometry explored with a single nuclear spin qudit, npj Quantum Inf. **4**, 1 (2018).

[10] P. R. Forrester, F. Patthey, E. Fernandes, D. P. Sblendorio, H. Brune, and F. D. Natterer, Quantum state manipulation of single atom magnets using the hyperfine interaction, Phys. Rev. B **100**, 180405(R) (2019).

[11] A. Płomińska and I. Weymann, Tunnel magnetoresistance of a supramolecular spin valve, Europhys. Lett. **125**, 18004 (2019).

[12] A. Gaita-Ariño, F. Luis, S. Hill, and E. Coronado, Molecular spins for quantum computation, Nat. Chem. **11**, 301 (2019).

[13] R. J. Blagg, L. Ungur, F. Tuna, J. Speak, P. Comar, D. Collison, W. Wernsdorfer, E. J. McInnes, L. F. Chibotaru, and R. E. Winpenny, Magnetic relaxation pathways in lanthanide single-molecule magnets, Nat. Chem. **5**, 673 (2013).

[14] M. A. Antunes, J. T. Coutinho, I. C. Santos, J. Marçalo, M. Almeida, J. J. Baldoví, L. C. Pereira, A. Gaita-Ariño, and E. Coronado, A mononuclear uranium (IV) single-molecule magnet with an azobenzene radical ligand, Chem. - Eur. J. **21**, 17817 (2015).

[15] S. Demir, I. R. Jeon, J. R. Long, and T. D. Harris, Radical ligand-containing single-molecule magnets, Coord. Chem. Rev. **289**, 149 (2015).

[16] K. L. Trojan, W. E. Hatfield, K. D. Kepler, and M. L. Kirk, Strong exchange coupling in lanthanide bis-(phthalocyaninato) sandwich compounds, J. Appl. Phys. **69**, 6007 (1991).

[17] K. L. Trojan, J. L. Kendall, K. D. Kepler, and W. E. Hatfield, Strong exchange coupling between the lanthanide ions and the phthalocyaninato ligand radical in bis (phthalocyaninato) lanthanide sandwich compounds, Inorg. Chim. Acta **198**, 795 (1992).

[18] D. Komijani, A. Ghirri, C. Bonizzoni, S. Klyatskaya, E. Moreno-Pineda, M. Ruben, A. Soncini, M. Affronte, and S. Hill, Radical-lanthanide ferromagnetic interaction in a Tb^{III} bis-phthalocyaninato complex, Phys. Rev. Materials **2**, 024405 (2018).

[19] L. Yang, X. Wang, M. Zhu, T. Xiao, Z. Ouyang, Y. Bian, Z. Wang, and J. Jiang, Ferromagnetic coupling between 4f and delocalized π-radical spins in mixed (phthalocyaninato)(porphyrinato) rare earth double-decker SMMs, Inorg. Chem. Front. **6**, 2142 (2019).

[20] S. Sanvito, Molecular spintronics, Chem. Soc. Rev. **40**, 3336 (2011).

[21] F. Troiani, C. Godfrin, S. Thiele, F. Balestro, W. Wernsdorfer, S. Klyatskaya, M. Ruben, and M. Affronte, Landau-Zener Transition in a Continuously Measured Single-Molecule Spin Transistor, Phys. Rev. Lett. **118**, 257701 (2017).

[22] L. Landau, Zur theorie der energieubertragung ii, Phys. Z. Sowjetunion **2**, 46 (1932).

[23] C. Zener, Non-adiabatic crossing of energy levels, Proc. R. Soc. London, Ser. A **137**, 696 (1932).

[24] E. Stuckelberg, Helv. Phys. Acta **5**, 36 (1932).

[25] E. Majorana, Atomi orientati in campo magnetico variabile, Nuovo Cimento **9**, 43 (1932).

[26] C. Godfrin, S. Thiele, A. Ferhat, S. Klyatskaya, M. Ruben, W. Wernsdorfer, and F. Balestro, Electrical read-out of a single spin using an exchange-coupled quantum dot, ACS Nano **11**, 3984 (2017).

[27] K. Hymas and A. Soncini, Mechanisms of spin-charge conversion for the electrical readout of 4f quantum states in a $TbPc_2$ single-molecule magnet spin transistor, Phys. Rev. B **102**, 045313 (2020).

[28] K. Hymas and A. Soncini, Origin of the hysteresis of magnetoconductance in a supramolecular spin-valve based on a $TbPc_2$ single-molecule magnet, Phys. Rev. B **102**, 125310 (2020).

[29] N. Ishikawa, M. Sugita, and W. Wernsdorfer, Quantum tunneling of magnetization in lanthanide single-molecule magnets: Bis (phthalocyaninato) terbium and bis (phthalocyaninato) dysprosium anions, Angew. Chem., Int. Ed. **44**, 2931 (2005).

[30] K. Blum, *Density Matrix Theory and Applications* (Springer Science & Business Media, 2012), Vol. 64.

[31] D. A. Garanin, in *Advances in Chemical Physics*, edited by S. A. Rice and A. R. Dinner (Wiley, Hoboken, NJ, 2012), Vol. 147.

[32] V. N. Golovach and D. Loss, Transport through a double quantum dot in the sequential tunneling and cotunneling regimes, Phys. Rev. B **69**, 245327 (2004).

[33] M. Ganzhorn, S. Klyatskaya, M. Ruben, and W. Wernsdorfer, Strong spin-phonon coupling between a single-molecule magnet and a carbon nanotube nanoelectromechanical system, Nat. Nanotechnol. **8**, 165 (2013).

[34] C. Godfrin, S. Lumetti, H. Biard, E. Bonet, S. Klyatskaya, M. Ruben, A. Candini, M. Affronte, W. Wernsdorfer, and F. Balestro, Microwave-assisted reversal of a single electron spin, J. Appl. Phys. **125**, 142801 (2019).

[35] H. Huang, W. V. D. Heuvel, and A. Soncini, Lanthanideradical magnetic coupling in $[LnPc_2]^0$: Competing exchange mechanisms captured via *ab initio* multi-reference calculations, Quantum Mater Res. **1**, e200003 (2020).

[36] P. Ao, Influence of Dissipation on the Landau-Zener Transition, Phys. Rev. Lett. **62**, 3004 (1989).

[37] P. Nalbach and M. Thorwart, Landau-Zener Transitions in a Dissipative Environment: Numerically Exact Results, Phys. Rev. Lett. **103**, 220401 (2009).

[38] P. Nalbach and M. Thorwart, Competition between relaxation and external driving in the dissipative Landau-Zener problem, Chem. Phys. **375**, 234 (2010).

[39] S. Javanbakht, P. Nalbach, and M. Thorwart, Landau-Zener quantum dynamics with transversal and longitudinal noise, Phys. Rev. A **91**, 052103 (2015).